Basics of Angle-Resolved Photoemission Spectroscopy

Tobias Helbig, MengXing Na, William Page, Kyle Wamer
(Dated: November 25, 2016)

I. INTRODUCTION

A wealth of information about the electronic structure of a material can be obtained through measurements of its photoelectrons—the electrons that are excited by incident photons and emitted into the vacuum by the photoelectric effect. The electronic energy states of the material can be probed by tuning the energy of the incident photons and by studying a range of photoelectron energies, as made clear in Eq. 1,

$$E_{kin} = h\nu - \phi - |E_B| \tag{1}$$

where E_{kin} is the photoelectron kinetic energy, $h\nu$ is the photon energy, ϕ is the material work function, and E_B is the electron binding energy inside the material.

The field of PhotoEmission Spectroscopy (PES) began in the relatively high energy range, using 1.5keV X-rays to explore the binding energies of core electrons in materials. Those experiments, conducted in the 1950s, successfully mapped out inner orbital energies of a variety of materials by only measuring the kinetic energy of the photoelectrons.[1] The clear peaks in their E_{kin} data corresponded to the binding energies of $1s$, $2s$, $2p$,... orbitals, and is illustrated by peaks labelled 'Core Levels' in Fig. 1).

PES has since branched into multiple sub-fields and techniques, and the one we focus on here is known for its relatively direct means of measuring valence electron dispersions in solids. The technique—Angular Resolved PhotoEmission Spectroscopy (ARPES)—is based on making precision measurements of both the photoelectrons' kinetic energies and their angular distribution. The momenta of the photoelectrons propagating in the vaccuum carry information about the electron momenta within the material, and are encoded in the photoelectrons' propagation angle in θ and ϕ. Thus by simultaneously measuring their kinetic energy and propagation angle, one can infer the momentum and energy of electrons in the material and thereby map out the electronic band structure—$E(\mathbf{k})$.[2] These dispersions are crucial for studying and explaining material properties. Some novel materials studied with this technique include unconventional superconductors, topological insulators, graphene, and more.

II. EXPERIMENTAL TECHNIQUE

ARPES begins with a light source - typically a laser or gas-discharge lamp that produces photons with energy high enough to overcome the work function of the material, and eject the electron with high E_kin. The work function of most materials are $3 - 6eV$, which lies in the ultraviolet range of the electromagnetic spectrum, so photons with energies in the range of $20 - 40eV$ are typically selected for ARPES. One of the most common sources is a helium lamp. In this source, a fraction of the helium gas is ionized and the positive ions are accelerated to the negative electrodes by an electric field. In the subsequent collisions, transfer of electrons between a neutral atom and an ion emit a discrete spectra of photons. A monochromator then selects the desired photon energy and sends it down the capillary towards the sample for photoemission.[3]

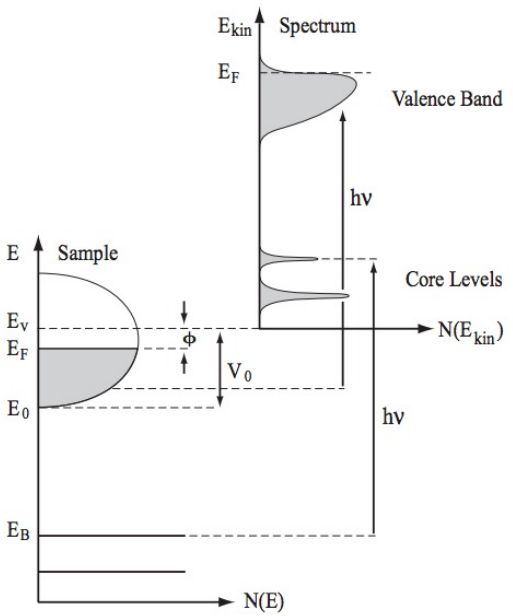

FIG. 1: Photoemmission energies - (lower left) valence bands and orbitals in the sample, with yet undefined variables E_0, the bottom of the valence band, and E_v, the vacuum level energy i.e. E_F + the work function. (upper right) example measured photoelectron spectrum.(source [2])

Electrons are emitted in all directions from the sample, and are collected by a nearby electronic lens that collimates the electron beam and decelerates it. The electrons are then sent to the hemispherical analyzer. The analyzer's slit selects the angular rat of the electrons collected, and the hemispherical capacitor's voltage can be tuned to select a specific range of energies. Electrons with too much or too little kinetic energy are absorbed by the walls, and do not make it to the multi-channel-plate (MCP) where the electrons are detected. The analyzer then backward-transforms the position of the electron on

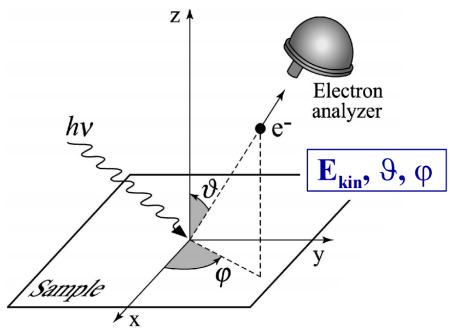

FIG. 2: Photoemission geometry - the angles θ and ϕ are defined with respect to the sample surface. The sample orientation on the mount is typically aligned via Laue diffraction.

the MCP to determine the energy of the electron as a function of the angular distribution. The angle information is related to the momentum by the following simple relations[2]:

$$\begin{aligned} k_x &= \frac{1}{\hbar}\sqrt{2mE_{kin}}\sin(\theta)\cos(\phi) \\ k_y &= \frac{1}{\hbar}\sqrt{2mE_{kin}}\sin(\theta)\sin(\phi) \\ k_z &= \frac{1}{\hbar}\sqrt{2mE_{kin}}\cos(\theta) \end{aligned} \tag{2}$$

The sample mount is equipped with movement in the x, y, and z directions, as well as rotation in θ and ϕ. These degrees of freedom can be used to determine the high symmetry points of the material. By mapping the energy at k_x and k_y, one can reconstruct the 3D electronic volume, the top face of which gives the fermi surface. Band structure can be obtained simply by taking cuts of the volume at particular k_x or k_y values.

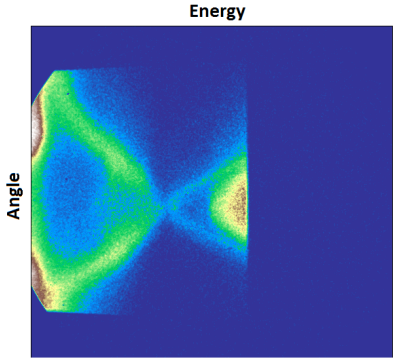

FIG. 3: Raw ARPES data of a topological insulator (bismuth selenide) taken with a helium lamp with 21eV photon energy, showing energy as a function of angle (θ). The top half of the Dirac cone - the surface states - are clearly visible, along with parts of the bulk conduction and valence bands. At 4K, the Fermi edge is sharp and can be used to determine the energy resolution of the system (approx. 2meV).

A. Experimental challenges and tr-ARPES

While ARPES is a powerful technique, it is an extremely sensitive one, and experimentally challenging to implement. The trajectory of the electrons are easily disturbed by extraneous fields, so the response function of electrons, which are often of interest, are beyond the abilities of this technique. Furthermore, photoelectrons are emitted generally within $1nm$ of the surface, so the surface of the sample must be kept extremely clean, which requires the sample to be cleaved in ultra-high-vacuum (UHV). Even at pressure levels of 10^{-11} torr, samples last no more than a few days, and the quality of the data degrades over this time frame. The flatness of the sample also limits the angular resolution of the data, this sometimes requires multiple cleaves, and no small amount of luck. To overcome this, a laser could be used instead of a lamp. The spot size of the laser is typically much smaller than that of the lamp, and gives better angular resolution when focused onto a "nice" place on the sample. Use of a laser is atypical, however, since it is difficult to make lasers with photon energies large enough to overcome the workfunction. Non-linear crystals can be used in sum-frequency generation to produce UV photons ($4eV$). However, although it is difficult, development of laser sources for ARPES is important, as it gives the ability to resolve electron dynamics in the material on time scales of $100fs$. Electronic relaxation dynamics provide a host of information about the material, and can find application in ultrafast optical control systems.

III. DATA ANALYSIS AND THEORY

A. Three step model

The photoemission process of one electron is evaluated as three separate processes:

1. Optical excitation of electron in the bulk of the material
2. Travel of the excited electron to the surface
3. Escape of electron to vacuum

The first step describes the total probability for an optical transition to occur due to the incident photon, and is dependent on the wavefunction overlap of the initial and final states. The second describes the scattering probability of an excited electron travelling to the surface by using an effective mean free path formalism. Lastly, the escape of the electron into vacuum is computed by the tunneling effect and depends on the energy of the excited electron and the material work function ϕ.

All relevant information about the band structure, which is of interest, is encoded in the first step, which is outlined in detail here. We begin by using Fermi's golden rule to compute the transition probability for the

optical excitation between the N-electron ground state Ψ_i^N and one of the possible final states Ψ_f^N :

$$\begin{aligned} w_{fi} &= \frac{2\pi}{\hbar} \cdot |\langle \Psi_f^N | H_{int} | \Psi_i^N \rangle|^2 \, \delta(E_f^N - E_i^N - h\nu) \\ \text{with } E_i^N &= E_i^{N-1} - E_B(\vec{k}) \\ \text{and } E_f^N &= E_f^{N-1} + E_{kin}. \end{aligned}$$

The perturbative Hamiltonian can be found by applying the minimal coupling of the electromagnetic field to the system and by neglecting the term proportional to $\vec{A}^2$:

$$H_{int} = \frac{e}{2mc}(\vec{A}\cdot\vec{p} + \vec{p}\cdot\vec{A}) = \frac{e}{mc}\vec{A}\cdot\vec{p}$$

In this Hamiltonian, we have fixed the $\Phi = 0$ gauge, and used the dipole approximation $\vec{\nabla}\cdot\vec{A} = 0$, in which the operators $\vec{A}$ and $\vec{p}$ commute. Although this assumption may not hold at the surface, it is a phenomenological description and works well in most experiments.

Our first goal is to rewrite the final state,

$$\Psi_f^N = \mathcal{A}\,\phi_f^{\vec{k}} \cdot \Psi_f^{N-1}.$$

The operator $\mathcal{A}$ is an antisymmetric operator which ensures that the Pauli principle is obeyed. The state $\Psi_f^{N-1} = \Psi_m^{N-1}$ is an excited state of the system with energy E_m^{N-1} and an eigenstate to the $(N-1)$-particle-Hamiltonian. In writing the final wavefunction this way we make use of the sudden approximation, which states that an electron is instantaneously removed from the system and the effective potential changed discontinuously. This approximation is generally valid for ARPES, in which the electron possesses sufficiently high energy to escape into the vacuum on time scales shorter than the system response time.

The initial state can be approximated using the Hartree-Fock formalism, in which we ignore interactions and write the wavefunction as the product of the photoemitted electron orbital $\phi_i^{\vec{k}}$ and the $(N-1)$-particle Slater determinant,

$$\Psi_i^N = \mathcal{A}\,\phi_i^{\vec{k}} \cdot \Psi_i^{N-1}.$$

It remains to note that Ψ_i^{N-1} is in general not an eigenstate to the (N-1)-particle Hamiltonian, because it can be displayed as $\Psi_i^{N-1} = c_{\vec{k}}\Psi_i^N$, where $c_{\vec{k}}$ is the one-particle annihilation operator for the momentum $\vec{k}$.

The full transition probability is then the sum over all possible final states and separates into a product of two parts,

$$w_{fi} = |M_{fi}^{\vec{k}}|^2 \cdot \sum_m |c_{mi}|^2 \, \delta(E_{kin} + E_m^{N-1} - E_i^N - h\nu)$$

and the measured intensity at the detector is therefore proportional to the total number of transitions made,

$$I(\vec{k}, E_{kin}) = \sum_{f,i} w_{fi} \tag{3}$$

which is a sum over all possible initial and final states. The final formula consists of the one-electron dipole matrix element $M_{fi}^{\vec{k}} = \langle \phi_f^{\vec{k}} | H_{int} | \phi_i^{\vec{k}} \rangle$ and the (N-1)-electron overlap integral $c_{mi} = \langle \Psi_m^{N-1} | \Psi_i^{N-1} \rangle$. The coefficients $|c_{mi}|^2$ can be interpreted as the probability that the removal of an electron from the initial state i leaves the (N-1)-particle system in an excited state m.

B. Data and modelling

Information about the band structure is encoded in the $|c_{m,i}|^2$ terms. We define

$$\begin{aligned} A^-(\boldsymbol{k},\omega) :=& \sum_m |c_{m,i}|^2 \delta(\omega - E_m^{N-1} + E_i^N) \\ =& \frac{1}{\pi} \frac{-\Sigma''}{[\omega - E_m^{N-1} + E_i^N - \Sigma']^2 + [\Sigma'']^2} \end{aligned} \tag{4}$$

where $\omega = h\nu - E_{\text{kin}} = \phi + |E_B|$ is the absolute value of the bound electron's energy (measured from the Fermi surface) before photoexcitation. This function A^- is called the *one-particle spectral function*, and is related to the imaginary part of the one-particle Green's function. It can also be written in terms of the electron's self energy Σ. (Details in Appendix.)

We can now write an expression for the ARPES intensity (what we measure in experiments)

$$I(\boldsymbol{k},\omega) = I_0(\boldsymbol{k},\nu,\boldsymbol{A}) f(-\omega) A^-(\boldsymbol{k},\omega) \tag{5}$$

where I_0 is proportional to the one-particle matrix elements, and the Fermi function $f(-\omega)$ ensures only states below E_F are photoexcited. The interesting behaviour comes from the spectral function A^-, since it is a sum of δ-functions.

We begin with the Hartree-Fock formalism, and approximate the electrons as non-interacting. Removing an electron then, leaves the system in an $(N-1)$-electron eigenstate (it will still be a Slater determinant). Taking the inner product, we see that only a single $c_{m,i}$ term is nonzero and $I(\boldsymbol{k},\omega) \propto \delta(\omega - |\epsilon_{\boldsymbol{k}}^b|)$, where $\epsilon_{\boldsymbol{k}}^b$ is the energy of the photoelectron excited from some band b (see LHS of III B). Repeating this process allows one to map out the entire band structure.

Adding electron-electron or el-ph interactions means that the final wavefunction will no longer be an eigenstate of the system. Taking the inner product give more than one non-zero $c_{m,i}$ coefficients, which amounts to a

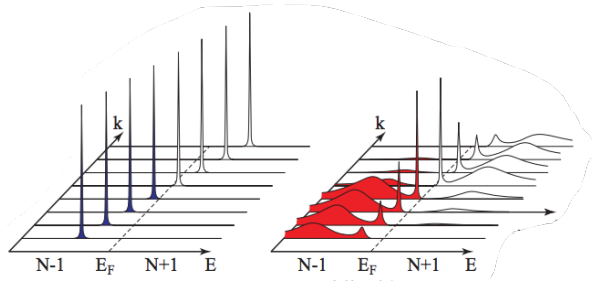

FIG. 4: LHS: Delta function spectrum of non-interacting electrons. RHS: Broadening of spectrum do to el-ph or el-el interactions. Notice a coherent 'main peak' remains.

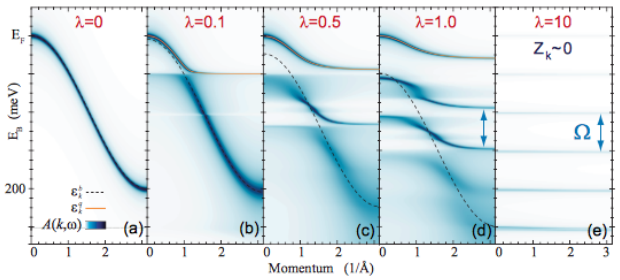

FIG. 5: Spectral function for various levels of el-ph coupling (λ) in 1D Holstein. The weight surrounding the quasiparticle band (top) is coherent; the remaining weight is incoherent.

broadening of the spectral function. However, if the notion of quasiparticle is still valid (i.e. Fermi liquid), we will still have a main peak. We call this the *coherent spectral weight*, while the *incoherent spectral weight* corresponds to everything else (see RHS of III B). The form of the coherent spectral weight is

$$A^-_{\text{coherent}}(\boldsymbol{k},\omega) = Z_{\boldsymbol{k}}\delta(\omega - |\epsilon_{\boldsymbol{k}}|) \tag{6}$$

where $\epsilon_{\boldsymbol{k}}$ is the energy of the Fermi liquid quasi particle and $Z_{\boldsymbol{k}}$ is the *quasiparticle strength*. This $Z_{\boldsymbol{k}}$ can be extracted from integrating over the intensity peak, and is a relatively good measure of the correlation in a given system.

$$Z_{\boldsymbol{k}} = \int A_{\text{coherent}}(\boldsymbol{k},\omega)d\omega \tag{7}$$

In practice, identifying the coherent piece of the spectrum depends on the nature of interactions. If $A_{\text{incoherent}}$ originates from gapped excitations, e.g. coupling between electrons and optical phonons, the coherent part is well separated from the incoherent tail, and the analysis is relatively easier (as shown in the Holstein example below). But if $A_{\text{incoherent}}$ is due to gapless excitations, e.g. electron-hole pair creation, the coherent part is harder to isolate. Other methods are required in this case and we briefly discuss this in the YBCO example below.

1. *Holstein Hamiltonian example*

Using many-body theory, one can calcualte A^- for the 1-D Holstein model, as done in [4].

$$\mathcal{H} = \sum_k \epsilon^b_k c^\dagger_k c_k + \Omega \sum_q b^\dagger_q b_q + \frac{g}{\sqrt{N}} \sum_{k,q} c^\dagger_{k-q} c_k (b^\dagger_q + b_{-q})$$

at various levels of the coupling $\lambda = g^2/2t\Omega$ (see Figure 5). Here $\epsilon^b_k = -2t\cos(ka)$. At $\lambda = 0$, we only have spectral weight, so that A^- exactly follows the bare electronic band ϵ^b_k. At $\lambda = .1$, the band is renormalized into a quasiparticle band ϵ^q_k; for $\omega >$ this band, we have incoherent weight that smears the $\lambda = 0$ spectral line. As $\lambda \to \infty$, the amount of coherent weight goes to zero and the notion of quasiparticle vanishes. We also see the phonon excitations as bands appearing below the quasi-particle band.

2. *YBCO cuprate*

When we have gapless excitations causing strong correlations, as in the high-T_c cuprates, we cannot find A^-_{coherent} by looking at the isolated, main peak. In YBCO – one of the most studied cuprates due to its high purity level – Z_k can be calculated using a combination of experiment and density functional theory (in the figure below, what is measured is the splitting between two cuprate bilayers). By doping the cuprate, electronic correlations can be weakened, so that Z_k increases. For low-doping, $Z_k \approx 0$, and the quasiparticle picture breaks down; but after sufficient doping, Z_k lifts and Fermi liquid theory can be applied. See references within [2] for sources of data.

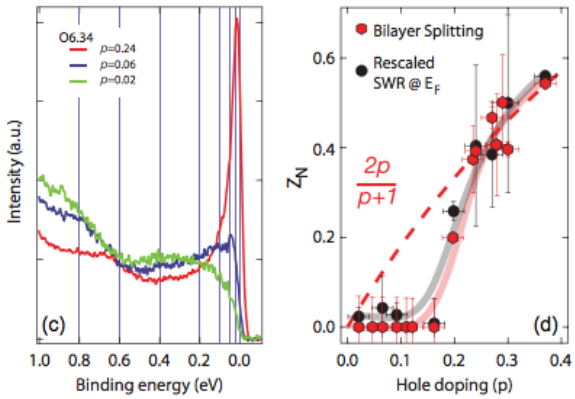

FIG. 6: (c): The spectral function A_-, at the Fermi surface, as a function of energy. (d): The coherence factor Z_k, at various levels of doping. Red is DFT calcaultion; Black is integration of A over 'main peak'

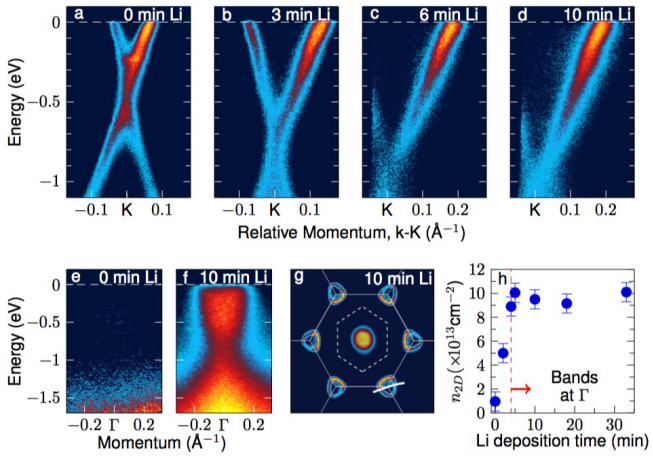

FIG. 7: (a-d) Electron dispersions at the Dirac cone K-point as a function of Li deposition duration. (e,f) Dispersions at the Γ point.(g) The graphene BZ, with the white line showing the k_x-k_y cut along which the K-point dispersions were measured. (h) The electron density at Γ as a function of deposition time. (source [7])

IV. ARPES AT UBC

With the preceding sections describing the ARPES measurement and analysis, this final section is meant to give a sense for where ARPES research currently stands. The ARPES apparatus at UBC is being used to better understand high-T_c cuprates, MgB_2, graphene, topological insulators, orbital-ordered ferromagnets, and other materials. We briefly describe induced superconductivity in graphene by the deposition of lithium adatoms, for which UBC has received recognition within the physics community.

In 2015 the UBC group found the first evidence for superconductivity in graphene via analysis of ARPES intensity spectra [6]. While pristine monolayer graphene does not exhibit superconductivity, it was proposed that lithium decorated on graphene would enhance the electron phonon coupling by introducing a strong coupling mode to in-plane lithium phonon modes. The ARPES spectra at the K point (fig 7 (a-d)) shows the Dirac point shift to higher binding energies for longer Li deposition times, indicating that the Li atoms electron dope the graphene. The increase of the graphene sheet carrier density (fig 7 (h)), calculated using the Γ point ARPES spectrum (fig 7 (e,f)), is in agreement with predictions of the carrier density for an ordered LiC_6 superstructure—the structure needed for the proposed superconducting mechanism.

A superconducting state can be achieved by introducing an attractive potential between electrons to overcome the Coulomb repulsion between them and to form bosonic Cooper pairs. These bosons form a condensate at the critical temperature and are protected from scattering by a superconducting gap. In conventional superconductors, this attractive potential is mediated by scattering of electrons with momentum $\vec{k}$ to $\vec{k}'$ by a phonon with momentum $\vec{q} = \vec{k}' - \vec{k}$, the strength of which is characterized by the el-ph coupling.

Because the ARPES intensity spectrum contains information about the *one-particle* spectral function, it can be fit for two superconducting parameters of interest: the el-ph coupling parameter λ, and the superconducting gap energy Δ. To first order, kinks in the K point dispersions (fig 7 (a-d)) indicate increased el-ph coupling; detailed fits show that the el-ph coupling is increased by up to a factor of 3 when monolayer graphene is decorated with Li atoms. To explore the possibility of non-zero Δ, ARPES data was also taken at temperatures above and below the predicted T_c of LiC_6. A temperature dependent gap was found that translates to $T_c = 5.9K$, in good agreement with theoretical predictions. Further discussion of Δ and λ fitting can be found in [7].

Conclusion

In conclusion, we hope this short report was able to illustrate the basic principles behind ARPES - to give a brief overview of it's theoretical foundations, experimental techniques, it's advantages, it's disadvantages, and how it can help us understand condensed matter systems. ARPES as a technique is under continuous development. Experiments are underway where ARPES chambers are designed to be used with a spin detector, or coupled to an ultrafast source. With an ever growing reservoir of materials to study, and the continuous refinement of the technique, ARPES promises to be a rich field of study for years to come.

[1] C. Nordling, E. Sokolowski, K. Siegbahn. (1957). Physical Review. 105(5): 1676.

[2] R. comin, A. Damascelli. (2013). Springer Series in Solid-State Sciences. **180** pp 31-71.

[3] C. Stieger. (2012) Semester-Thesis. http://n.ethz.ch/ stiegerc/Semesterarbeit$_C$*hristian*$_f$*inal.pdf*

[4] C.N. Veenstra, G.L. Goodvin, M. Berciu, A. Damascelli. (2011). Phys. Rev. B **84**, 085126.

[5] G.D. Mahan. (2011) *Many-Particle Physics.* Plenum Press, New York.

[6] B.M. Ludbrook *et al.* (2015). PNAS **112**(38).

[7] B. M. Ludbrook. UBC thesis. (https://open.library.ubc.ca/cIRcle/collections/ ubctheses/24/items/1.0135608)

V. APPENDIX

Green's Functions

Below we briefly outline the relationship between the sceptical function $A^-(k,\omega)$, and the one-particle Green's function. First, a definition: The time-ordered one-particle Green's function is

$$G(\lambda, t-t') = -i\langle GS|Tc_\lambda(t)c_\lambda^\dagger(t')|GS\rangle$$

where λ are the quantum numbers of interest. When $\lambda = x$ is the position of the electron, the c_λ are field operators $\psi(x)$. We will be using $\lambda = \{k,\sigma\}$. This expression is true only at zero temperature; at finite temperature, we must take a thermal average. When the GS is a Fermi sea, and $\lambda = k,\sigma$. Now, $G(\lambda, t-t')$ is the probability amplitude that a state created at t' will be in the same state after $|t-t'|$. The time ordering implies that if $t' > t$, we remove an electron instead.

In ARPES, we are interested in electron removal of an N-particle ground state ψ_i^N, so we want:

$$-i\langle\psi_i^N|c_\lambda^\dagger(t')c_\lambda(t)|\psi_i^N\rangle$$

which we get for $t < t'$ from the above expression. Now, $\langle\psi_i^N|c_\lambda^\dagger(t')$ will be an $N-1$ particle state, which we can write in terms of a complete basis of states ψ_m^{N-1}:

$$\langle\psi_i^N|c_\lambda^\dagger = \sum_m \langle\psi_i^N c_\lambda^\dagger|\psi_m^{N-1}\rangle\langle\psi_m^{N-1}|$$

(It is not simply ψ_i^{N-1}, since some time $t'-t$ has elapsed) and our Green's function becomes

$$G(\lambda, t<t') = -i\sum_m |\langle\psi_m^{N-1}|c_\lambda(t-t')|\psi_i^N\rangle|^2$$

[Here we've removed the time dependence of the state ψ_m^{N-1} by shifting t by t']. Since energy is a more useful description of the particle than its time of propagation, we Fourier transform to get

$$G(\omega,\lambda) = \int_0^\infty dt e^{i\omega t}G(\lambda,t)$$

Now, we expand we each term:

$$-i\langle\psi_m^{N-1}|c_\lambda(t-t')|\psi_i^N\rangle =$$

$$-i\langle\psi_m^{N-1}|e^{iH(t-t')}c_\lambda e^{-iH(t-t')}|\psi_i^N\rangle =$$

$$-ie^{i(E_m^{N-1}-E_i^N)(t-t')}\langle\psi_m^{N-1}|c_\lambda|\psi_i^N\rangle$$

We can Fourier transform these quantities, remembering their is an implicit $\theta(t'-t)$ term here.

$$-i\int dt e^{i\omega(t'-t)}e^{i(E_m^{N-1}-E_i^N)}\theta(t'-t) =$$

$$\frac{1}{\omega - E_m^{N-1} + E_i^N - i\eta}$$

where $\eta \ll 1$ is included for regularization. Using this for each term in the summation over m, we have

$$G(\omega,\lambda) = \sum_m \frac{|\langle\psi_m^{N-1}|c_\lambda(t)|\psi_i^N\rangle|^2}{\omega - E_m^{N-1} + E_i^N - i\eta}$$

This resembles our spectral function [reference to equation in report], except we have $1/x$ structure instead of $\delta(x)$ structure. To fix this, we use the fact that

$$\lim_{\eta\to 0}\frac{1}{x-i\eta} = \mathcal{P}\frac{1}{x} + \frac{1}{\pi}\delta(x)$$

So that

$$A^- := \frac{1}{\pi}\mathrm{Im}G(\omega,\lambda) = \sum_m |\langle\psi_m^{N-1}|c_\lambda(t)|\psi_i^N\rangle|^2\delta(\omega - E_m^{N-1} + E_i^N)$$

To reiterate, at nonzero temperature, we must make a thermal average over the RHS.

Self Energy

Many-body theory tells us that when interactions are involved, the removed electron energy E_m^{N-1} gets shifted by a complex self-energy function, Σ:

$$G(\lambda_m,\omega) =$$

$$\frac{1}{\omega - E_m^{N-1} + E_n^i - i\eta} \mapsto \frac{1}{\omega - E_m^{N-1} + E_n^i - i\eta - \Sigma(\lambda,\omega)}$$

To read off the imaginary part, we write $\Sigma = \Sigma' + i\Sigma''$, so

$$A^- = \frac{1}{\pi}\frac{-\Sigma''}{[\omega - E_m^{N-1} + E_i^N - \Sigma']^2 + [\Sigma'']^2}$$

Now, instead of a divergence at the removal energy $E_m^{N-1} - E_i^N$, the peak is softened by the imaginary part of the self energy. Moreover, the location of the peak is shifted by the real part of the self-energy. In fact, the coherence factor Z_k we defined above is proportional to Σ''. By calculating Σ (to some order in perturbation theory), we can obtain a theoretical expression for Z_k.